Yukawa model on a lattice in the quenched approximation

Feliciano de Soto[*]
Departamento Sistemas Físicos, Químicos y Naturales, U. Pablo de Olavide, 41013 Sevilla, Spain

Jean-Christian Anglès d'Auriac[†]
Institut Neel, 25 Avenue des Martyrs, Boîte Postale 166, Grenoble 38042, France and
Laboratoire de Physique Subatomique et Cosmologie, 53 Avenue des Martyrs, Grenoble 38026, France
(Received 9 December 2011; revised manuscript received 12 March 2012; published 13 April 2012)

The Yukawa model in the quenched approximation is expressed as a disordered statistical mechanics model on a four-dimensional Euclidean lattice. We study this model, giving particular attention to the singularities of the Dirac operator in the phase diagram. A careful analysis of a particular limiting case shows that finite volume effects can be huge and questions the quenched approximation. This is confirmed by numerical simulation performed in this limiting case and without the quenched approximation.

DOI: 10.1103/PhysRevE.85.041121 PACS number(s): 05.50.+q, 11.15.Ha

I. INTRODUCTION AND MODEL

A. Introduction

For a long time it has been recognized that quantum field theory can be expressed as a statistical mechanics problem. The two areas have benefited from their proximity and many techniques developed in one context have been used in the other [1]. The expression of quantum field theories in terms of statistical mechanics has been especially useful in the context of the fundamental theory describing the interaction of quarks and gluons, i.e., quantum chromodynamics (QCD), where the usual perturbative techniques fail. Indeed it has been found that perturbative series in any quantum field theory have a zero convergence radius and are asymptotic but never convergent [2]. In such situations, it is common to resort to a numerical approach based on the Feynman path-integral formulation, where the system is described by a discretized action on a space-time lattice [3].

The numerical formulation of QCD on a lattice is currently among the most challenging problems in numerical physics and the progress made during past decades has been very important. The methods developed in this context can also be applied to other quantum field theories [4] in situations where perturbation theory fails, for example in the investigation of binding energies. Indeed such calculations would require the evaluation of an infinite number of contributions in a perturbative scheme.

In this paper we study the simplest fermion quantum field theory in four space-time dimensions, that is, the model introduced by Yukawa for the nuclear interaction [5]. The model is described in detail in Ref. [6], but since the aim of this paper is to adopt a statistical mechanics point of view, we use a schematic approach to illustrate how one goes from nuclear physics modeling to the statistical mechanics formulation.

Similar models were analyzed some time ago using the same techniques [7], and two distinct regimes were found: for small and large values of the coupling constant the system was numerically solvable, whereas for intermediate values it was not. In this paper we address this issue in detail (see also Ref. [6]). The same techniques have been used for a numerical study of a similar model [8], where bounds on the Higgs boson mass are established based on a Yukawa coupling between quarks and the Higgs boson.

B. The model

The model introduced by Yukawa aimed at a description of nuclei via the exchange of particles in analogy with quantum electrodynamics, except that the particles mediating the nuclear force have to be massive in order to have a finite range interaction. Although it is accepted that QCD is the fundamental theory of quarks and gluons responsible for nuclear interactions, one-boson exchange models are still mandatory in the nuclear physics community.

Therefore, in the Yukawa model, nucleons and mesons are considered elementary particles (i.e., without an internal structure), represented by local fields. The mesons are bosons represented by a real scalar field ϕ while nucleons are fermions represented by a four-component Grassmannian Dirac spinor ψ. To get a statistical mechanics model one works in a Euclidean space instead of in a Minkowski space; this is achieved by performing a Wick rotation [9] and the space-time is discretized into a four-dimensional hypercubic lattice. One possible choice for the discretized action [9] is

$$S = \frac{1}{2}\sum_x \left[(8+\mu^2)\phi_x^2 - 2\sum_\nu \phi_x\phi_{x+\nu}\right] + \sum_x \bar{\psi}_x D_{\mathrm{W}}\psi_x + g\sum_x \bar{\psi}_x\phi_x\psi_x, \quad (1)$$

which is the sum of three terms, $S = S_{\mathrm{KG}} + S_{\mathrm{W}} + S_{\mathrm{I}}$. In the first term, which is just a Klein-Gordon action for a free bosonic field, x runs over the N sites, ν runs over the four space-time directions, and μ is the meson mass. The second term is bilinear in the Dirac-Wilson operator D_{W}. It is a $4N \times 4N$ matrix, with elements

$$(D_{\mathrm{W}})_{x\,y} = 1_4\delta_{x,y} - \kappa\sum_\nu[(1_4+\gamma_\nu)\delta_{x,y-\nu} + (1_4-\gamma_\nu)\delta_{x,y+\nu}], \quad (2)$$

[*]fcsotbor@upo.es
[†]dauriac@grenoble.cnrs.fr

where 1_4 is a 4×4 unity matrix and γ_ν are the Dirac matrices ($\bar{\psi}$ is the conjugate of ψ), and κ is the so-called hopping parameter related to the bare fermion mass by the relation $M = 1/\kappa - 8$. The coupling between the two fields is realized in the simplest way by the third term, where g is the coupling constant. Every dimensional quantity has been redefined in terms of the lattice spacing a; therefore, the model depends on the three dimensionless lattice parameters g, μ, and κ. It depends also on the size of the lattice. In this work we use periodic boundary conditions and take the four dimensions to be equal.

Propagators in quantum field theory are expressed using Wick contractions. From the statistical mechanics point of view, this amounts to computing expectation values and to combining them together. For example the elementary fermion propagator reads

$$S(x,y) = \frac{1}{Z}\int [d\phi](D(\phi)^{-1})_{xy}\det(D(\phi))e^{-S_{\mathrm{KG}}(\phi)}, \quad (3)$$

where x and y are two sites of the lattice and

$$D(\phi) = D_{\mathrm{w}} + g\phi \quad (4)$$

is the interacting Dirac operator; Z is the normalization factor of the field probability distribution and it is not calculated in practice. Propagators like (3) provide a simple way of computing the renormalized mass m of an interacting particle in quantum field theory (QFT), as

$$C(x_4) = \sum_{x_1,x_2,x_3} S(x,0) \sim \cosh m\left(\frac{L}{2} - x_4\right), \quad (5)$$

where x_4 is the time coordinate. The calculation of renormalized masses is performed by producing the fields ϕ_x according to a joint probability distribution

$$\Pi(\{\phi_x\}) \sim \det(D(\phi))e^{-S_{\mathrm{KG}}(\phi)} \quad (6)$$

and computing $S(x,0)$ as the average over field configurations of $(D(\phi)^{-1})_{0x}$. Note that it implies solving a linear system, not a full inversion of the Dirac operator.

In the boson probability distribution Eq. (6), the evaluation of the fermionic determinant is largely the most expensive part of the calculation. Sophisticated methods have been developed for dealing with this difficulty, such as hybrid Monte Carlo simulations [10], but the study of the model neglecting the effect of the determinant on the weight of the field configuration, called the quenched approximation, yet deserves interest and is described in some detail in the next section. Finally, let us remind that to extract physical quantities one needs to be as close as possible to a critical point so that the operator $D(\phi)$ has low modes. This implies the same numerical difficulties as in the vicinity of any critical point.

C. Symmetries

In this section we review some of the symmetries of particular interest for the numerical treatment of the theory. The model exhibits some properties characteristic of a free theory that are preserved in the interacting case due to the structure of the interacting part of the action, Eq. (4).

First, for the free Dirac operator, it is possible to find an involution J, satisfying

$$D = JD^{\star}J, \quad (7)$$

with $J = i\gamma_1\gamma_3$ in the Dirac γ-matrix representation [9]. This property holds in the interacting case since the interaction term is real and diagonal in spinor space. The inverse S of the Dirac operator also has the same property. Therefore, for any field configuration, the fermion propagator has the following form:

$$S(x) = \begin{pmatrix} a & b & c & d \\ -b^{\star} & a^{\star} & -d^{\star} & c^{\star} \\ e & f & g & h \\ -f^{\star} & e^{\star} & -h^{\star} & g^{\star} \end{pmatrix}. \quad (8)$$

This implies that we must solve two (and not four) independent linear systems for each fermion propagator. This symmetry does not hold for QCD or, in general, for interacting theories with a different spinor structure.

There is another simplification due to the fact that the interaction term is diagonal in spinor space; i.e., it commutes with all the γ matrices. For the free case, when a reflection is performed on one direction, $x_k \to -x_k$, while keeping the other coordinates fixed, the Dirac operator transforms as (see Sec. 8.2 of Ref. [1])

$$D \to \gamma_5\gamma_k D\gamma_k\gamma_5.$$

This property also holds for its inverse, S. The Yukawa coupling term preserves this symmetry.

As the action is invariant under any permutation belonging to the automorphic group of the lattice (and, in particular, a reflection over one coordinate), the probability of a given configuration is the same after performing a reflection. Using this relation the time correlator (5) after averaging over meson configurations takes the form

$$C(x_4) = \sum_{x_1,x_2,x_3} S(x_4) = \begin{pmatrix} c(x_4) & 0 & 0 & 0 \\ 0 & c(x_4) & 0 & 0 \\ 0 & 0 & c(L_4 - x_4) & 0 \\ 0 & 0 & 0 & c(L_4 - x_4) \end{pmatrix}. \quad (9)$$

Note that C depends on a single function $c(x_4)$ instead of on 16 functions.

D. The quenched approximation

The quenched approximation consists of neglecting the variation of $\det(D(\phi))$ among the field configurations. From a physical point of view, this determinant accounts for the creation of virtual nucleon-antinucleon pairs, and its effect is expected to be small as long as the meson mass is smaller than the nucleon one. It simplifies considerably the problem since now Eq. (6) becomes

$$\mathrm{Prob}(\{\phi_x\}) \sim \exp\left(-\frac{1}{2}\sum_x\left[(8+\mu^2)\phi_x^2 - 2\sum_\mu \phi_{x+\mu}\phi_x\right]\right). \quad (10)$$

This distribution no longer involves the Dirac operator and is easy to implement. Indeed the quadratic form, argument of the exponential, can be diagonalized straightforwardly, simply by going to the discrete Fourier space. We denote $\tilde{\phi}_k$ the Fourier transform of ϕ_x. The $\tilde{\phi}_k$ are complex and their joint probability factorizes as

$$\mathrm{Prob}(\{\tilde{\phi}_k\}) \sim \prod_k \exp\left(-\frac{1}{2}\frac{|\tilde{\phi}_k|^2}{\sigma_k^2}\right) \tag{11}$$

with $\sigma_k^2 = \frac{1}{\mu^2+\sum_\nu \hat{k_\nu}^2}$, where $\hat{k_\nu} = 2\sin\frac{k_\nu}{2}$ with the extra constraint $\tilde{\phi}_k^\star = \tilde{\phi}_{-k}$ in order to get real values for ϕ_x. It is then simple to draw independently the real and imaginary parts of each $\tilde{\phi}_k$ (for $k > 0$) from a centered Gaussian distribution with variance σ_k^2. The partial distribution of ϕ_x (i.e., integrating out all ϕ_y but ϕ_x) is also a Gaussian with a variance σ independent of x and given by

$$\sigma^2(\mu) = \frac{1}{N}\sum_k \sigma_k^2 = \frac{1}{N}\sum_k \frac{1}{\mu^2 + \sum_\nu \hat{k_\nu}^2}. \tag{12}$$

In summary ϕ_x are Gaussian dependent random variables with the same variance whereas $\tilde{\phi}_k$ are independent with a variance depending on k. Note that generating uncorrelated configurations is automatic with the method presented above.

II. THE DIRAC OPERATOR SPECTRUM IN THE PHASE SPACE κ-g

Let us recall that the model depends on three independent parameters, κ, g, and μ. As shown above, in the *quenched approximation* the probability of ϕ_x depends only on μ and not on κ or g; it is the same everywhere in the parameter space. In this section we work with a constant value of $\mu \sim 0.1$.

Any numerical computation of a physical quantity will imply some inversions of the Dirac operator, Eq. (4). We know that this inversion will have to be performed with values of g and κ such that the linear system is difficult to invert. In practice, in some region of the g-κ plane and for a given value of the linear sizes of the lattice, solving for X for the system $DX = Y$ is not possible. Indeed, depending on the numerical method used, either the algorithm will not converge or it will find a wrong solution. To quantify how ill conditioned the linear system is, it is customary to use the condition number. By definition a condition number measures how the solution of the system changes when the right-hand-side (RHS) term changes [11]. With the appropriate choice of the norm, the condition number is the ratio $r = \frac{|\lambda_a|}{|\lambda_i|}$ of the largest to the smallest moduli of the eigenvalues. With this definition, and for the type of system we consider, a system can be inverted reasonably if the condition number is smaller than $100 \sim 1000$. Note, however, that a condition number can be arbitrarily large but still the system is invertible. This is the case if the RHS of the system is in the kernel of the operator. This situation occurs with some preconditioning.

We now note that, due to the specific form of the Dirac operator in Eq. (4), one has

$$D(\alpha g, \alpha\kappa; \phi_x) - 1 = \alpha(D(g,\kappa;\phi_x) - 1), \tag{13}$$

where 1 denotes the $4N \times 4N$ unity matrix. Since the probability of the ϕ_x's does not depend on g and κ, one is led to introduce the polar coordinates r and θ of the parameter space $g = r\cos(\theta), \kappa = r\sin(\theta)$. For a given value of θ the spectrum of D evolves straightforwardly: the eigenvectors are then left unchanged and the eigenvalues λ_k evolve according to

$$\lambda^k(r,\theta) = \frac{r}{r_0}\lambda^k(r_0,\theta) + 1 - \frac{r}{r_0}. \tag{14}$$

In a spectral decomposition of D, varying r only changes the relative weights of the eigensubspaces. The value of θ fixes the spectrum, and the value of r fixes the relevant part. In general the eigenvalues are complex: $\lambda^k = \lambda^k_{\mathrm{Re}} + \imath\lambda^k_{\mathrm{Im}}$. Let us give a fixed value to θ and denote the spectrum $\lambda^k(r)$. We choose a reference value r_0 (one can take, for example, $r_0 = 1$) and note $\Lambda^k = \lambda^k(r_0)$; we have

$$|\lambda^k(r)|^2 = \left(|\Lambda^k|^2 - 2\Lambda^k_{\mathrm{R}} + 1\right)r^2 + 2\left(\Lambda^k_{\mathrm{R}} - 1\right)r + 1. \tag{15}$$

So the modulus of each eigenvalue is a parabola as a function of r. All these parabola intersect at the point $(r = 0, \lambda = 1)$. They also intersect each other at other points, and the two extremal eigenvalues change when r changes (see Fig. 1). The eigenvalue labeled by k will reach its smallest value

$$m_k = \frac{\left(\Lambda^k_{\mathrm{I}}\right)^2}{|\Lambda^k|^2 - 2\Lambda^k_{\mathrm{R}} + 1} \tag{16}$$

for $r = \frac{\Lambda^k_{\mathrm{R}} - 1}{|\Lambda^k|^2 - 2\Lambda^k_{\mathrm{R}} + 1}$. Therefore, only the eigenvalues with $\Lambda^k_{\mathrm{R}} < 1$ and $\Lambda^k_{\mathrm{I}} \ll 1$ give rise to a small denominator in the condition number. When $r \simeq 0$ the eigenvalue of lowest (largest) modulus will be the one with the smallest (largest) value of $\Lambda_{\mathrm{R}} - 1$; therefore, the condition number increases continuously from the value 1. In the other limit, $r \gg 1$, the eigenvalue of lowest (largest) modulus will be the one with the smallest (largest) value of $|\Lambda^k|^2 - 2\Lambda^k_{\mathrm{R}} + 1$, and the condition number tends to a finite value (the ratio of the two values above). In the intermediate regime, the condition number has very complicated behavior with a lot of maxima and minima. We analyze this behavior is the next sections for different cases.

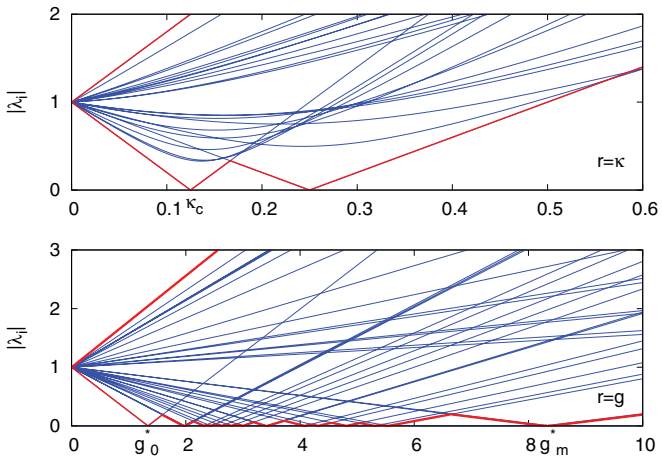

FIG. 1. (Color online) Evolution with r of the eigenvalue modulus for the two limiting cases $g = 0$ (top) and $\kappa = 0$ (bottom). In both cases only a selection of eigenvalues is shown for clarity. For $\kappa = 0$ a field configuration is generated according to Eq. (10). The largest and smallest moduli of the eigenvalues as a function of r are shown as a thick red line.

A. Case $\theta = \frac{\pi}{2}$

This corresponds to $g = 0$ and therefore this is the trivial case of *noninteracting* fermions; it is included for illustrative purposes. The evolution of the spectrum of D for Wilson discretization as a function of $r = \kappa$ is well known and has the form of Eq. (14): $\lambda_k = (1 - 2\kappa \sum_\nu c_\nu) \pm 2\kappa\imath\sqrt{\sum_\nu s_\nu^2}$ with $c_\nu = \cos(k_\nu)$ and $s_\nu = \sin(k_\nu)$. Therefore, the condition number behaves as

$$c(r=\kappa) = \begin{cases} \frac{1+8\kappa}{1-8\kappa} & \kappa < \frac{1}{8} \\ \frac{1+8\kappa}{8\kappa-1} & \frac{1}{8} < \kappa < \frac{1}{6} \\ \frac{1+8\kappa}{1-4\kappa} & \frac{1}{6} < \kappa < \frac{1}{4} \\ \frac{1+8\kappa}{4\kappa-1} & \frac{1}{4} < \kappa < \frac{1}{2} \\ 1+8\kappa & \frac{1}{2} < \kappa \end{cases}.$$

The condition number diverges at the values $\kappa = \frac{1}{8}$, corresponding to $k = (0,0,0,0)$, and $\kappa = \frac{1}{4}$, corresponding to $k = (\frac{L_1}{2},0,0,0)$ (or a permutation when the corresponding L_ν are even). The first value, $\frac{1}{8}$, is the critical value, whereas the other is unphysical since it corresponds to a negative mass.

This is compatible with the framework presented in the introduction of this section. For example, Eq. (16) becomes $m_k = \frac{\sum s_\nu^2}{(\sum c_\nu)2+\sum s_\nu^2}$. In the top graph in Fig. 1 the evolution of some eigenvalues with $r = \kappa$ is presented. One sees that for zero, eigenvalues appear only for $r = \frac{1}{8}$ and $r = \frac{1}{4}$.

B. Case $\theta = 0$

This case corresponds to $\kappa = 0$ and describes infinitely heavy fermions. It is unphysical but nontrivial. However, it is instructive to study it from a statistical mechanics point of view; also, if some continuity is to apply, it should not be very different from the small-θ case. In that case the Dirac operator is simply diagonal and the 4×4 blocks are given by

$$(D(\phi))_{x\,y} = (1 + g\phi_x)\delta_{xy}\,1_4. \tag{17}$$

Obviously the eigenvalues $1 + g\phi_x$ are all degenerated four times and *real*. Equation (15) becomes simply $[\lambda^k(r)]^2 = [1 + r(\Lambda^k - 1)]^2$. Since $\lambda^k(r)$ is linear with r, for any eigenvalue $\Lambda^k < 1$ there will be a value of r^k for which $\lambda(r^k) = 0$. This is the worst situation since for any field configuration the determinant of the Dirac operator will exactly vanish $\frac{N}{2}$ times. This is illustrated in Fig. 1, where all the eigenvalues as a function of g are shown. The two eigenvalues of largest and lowest moduli are emphasized. One clearly sees that the eigenvalue of the lowest modulus vanishes for many values of r (recall that $r = g$ when $\kappa = 0$). This situation is in contrast with the previous case, $\theta = \frac{\pi}{2}$, where the eigenvalue of lowest modulus vanishes only twice (for $r = \frac{1}{8}$ and $r = \frac{1}{4}$). There the eigenvalues are "protected" by their imaginary part.

In other words, the ϕ_x are N correlated real random variables following the probability distribution, Eq. (10), and we evaluate the condition number $c(r)$, which is in that case

$$c(r;\phi) = \frac{\max|1 + r\phi_x|}{\min|1 + r\phi_x|}. \tag{18}$$

Let us suppose that ϕ_x have been sorted in ascending order. We note λ_m, the largest negative eigenvalue. Since N is very large, we assume $m \sim \frac{N}{2}$ and there is at least one negative and one positive eigenvalue. Figure 1 illustrates the behavior of the spectrum of the Dirac operator for a given ϕ_x realization. Each eigenvalue varies linearly with g. Therefore, the condition number is controlled by the eigenvalue of smallest modulus, which is a piecewise linear function of g. The selected eigenvalue changes each time g reaches a value $g_i = -\frac{2}{\phi_i+\phi_{i+1}}$, and reaches zero for $g_i^\star = -\frac{1}{\phi_i}$ for $0 \leqslant i \leqslant m$, for which $g_0^\star < g_0 < g_1^\star < g_1 < \cdots$. Consequently three regimes occur. First, when $g < g_0^\star$ the condition number is a continuous increasing function of g (homographic) which diverges at g_0. Second, in the intermediate regime $g_0^\star < g < g_m^\star$ the condition number varies extremely fast, diverging m times. Finally, for $g_m^\star < g$ the condition number decreases homographically, saturating at a finite value. This is illustrated in Fig. 1 where the extreme values $g_0^\star$ and $g_m^\star$ are indicated.

In order to perform an analytical evaluation of those three regimes, we simplify the problem by choosing the fields ϕ_x *independent* with zero mean and a variance given by Eq. (12). It turns out that this simplification does not change substantially the average value of the eigenvalue of lowest modulus, as illustrated in Fig. 2. This figure shows, among other things detailed below, the two curves of the eigenvalues of lowest modulus (curves labeled $N = 131\,072$) as a function of r when ϕ_x are independently and identically distributed Gaussian variables and when they are dependent: the two curves are completely indistinguishable. Within this assumption, when the number N of lattice sites increases, ϕ_m goes to zero as

$$\langle\phi_m\rangle = -\sigma\int_0^\infty \left(1 - \mathrm{erf}\frac{x}{\sqrt{2}}\right)^N dx \sim -\sigma\sqrt{\frac{2}{\pi}}\frac{1}{N}. \tag{19}$$

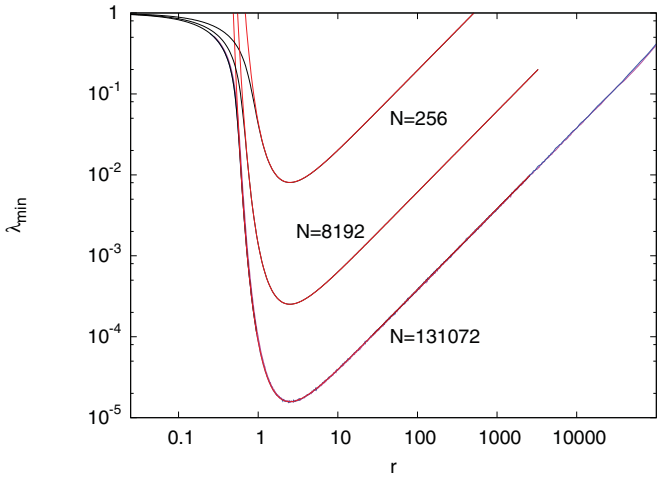

FIG. 2. (Color online) Smallest modulus of the eigenvalues vs g for $\kappa = 0$ and three values of L. For any value of L the numerical integration (black) together with the approximation (red) Eq. (A1) are shown. For the largest size $L = 32 \times 16^3$ the result of a simulation averaged over 8692 samples is also shown for both correlated ϕ_x (magenta line) and uncorrelated ϕ_x (dashed blue line). Actually the curves are indistinguishable except for at small $g < 1$, when the approximation of the integral is not correct.

Therefore, $g_m^\star \sim N$ and the third region shrinks when the lattice size increases. In other words the decreasing of the condition number for large values of the coupling constant g at $\kappa = 0$ is a size effect. On the other limit for small g, the first region, $g < g_0^\star$, is delimited by the smallest field ϕ_0 whose average is given by

$$\langle \phi_0 \rangle = -\sigma \int_0^\infty \left[1 - \left(\mathrm{erf} \frac{x}{\sqrt{2}} \right)^N \right] dx. \tag{20}$$

We see that $\langle \phi_0 \rangle$ diverges extremely slowly with N. To have $\langle \phi_0 \rangle$ of the order of ξ, one needs a huge lattice of $N \sim \xi \exp \frac{\xi^2}{2}$ sites. Therefore, the first region also disappears in the thermodynamic limit. However, this size effect will never be seen in an actual computation. Finally, we conclude that only the second region survives the large lattice volume. Let us recall that in this region and for any field configuration there are $m \sim \frac{N}{2}$ values of r for which one eigenvalue of the Dirac operator is exactly zero.

In the preceding paragraph the behavior of the condition number for a *given* configuration of ϕ_x has been studied. We need now to perform an average over the realization of ϕ_x. For a fixed value of g, different field configurations will give very different condition numbers, some of them possibly extremely large. Note, however, that the condition number is not a physical observable; it is only an indicator of how difficult the inversion will be. Therefore, the most probable value of the condition number may be more sensible. From the probability distribution of ϕ_x one can easily compute the average of the smallest and largest eigenvalues as a function of g. We show in the Appendix that

$$\langle |\lambda_i| \rangle \sim \frac{1}{N} \sqrt{\frac{\pi}{2}} g\sigma \ \exp \frac{1}{2g^2\sigma^2}, \tag{21}$$

$$\langle |\lambda_a| \rangle \lesssim g\sigma \sqrt{2 \ln N}, \tag{22}$$

where σ depends on μ and is given by Eq. (12). The eigenvalue of lowest modulus goes to zero as $\frac{1}{N}$ but the prefactor increases extremely fast when g goes to zero. Since N goes to infinity first, for any nonzero g, $\langle |\lambda_i| \rangle$ goes to zero. The eigenvalue of lowest modulus increases very slowly with N. This is illustrated in the lower part of Fig. 6, where we show the eigenvalue of lowest modulus for several lattice volumes. In this figure and for $N = 6432^3 = 131\,072$ we have plotted the result of a "genuine" simulation with dependent fields, another simulation with independent fields, a numerical integration of Eq. (A1), and the approximation Eq. (21). The agreement among these four calculations is excellent. We have also plotted the eigenvalue of lowest modulus for other values of N to show the size effects.

The appearance of the three regions described above can be seen in Fig. 3. In this figure we have plotted the average condition number $\langle \frac{|\lambda_{\max}|}{|\lambda_{\min}|} \rangle$ over 8692 samples as a function of g. The number of peaks is even larger with a smaller discretization of g. The quantity $\frac{\langle |\lambda_{\max}| \rangle}{\langle |\lambda_{\min}| \rangle}$ is much smoother since $\langle |\lambda_{\min}| \rangle$ never vanishes and also displays the three regimes. Moreover, in the *quenched* approximation it makes sense to consider a particular realization since the weight of a consideration does depend only on μ; we therefore have plotted a typical configuration. Finally, we have also

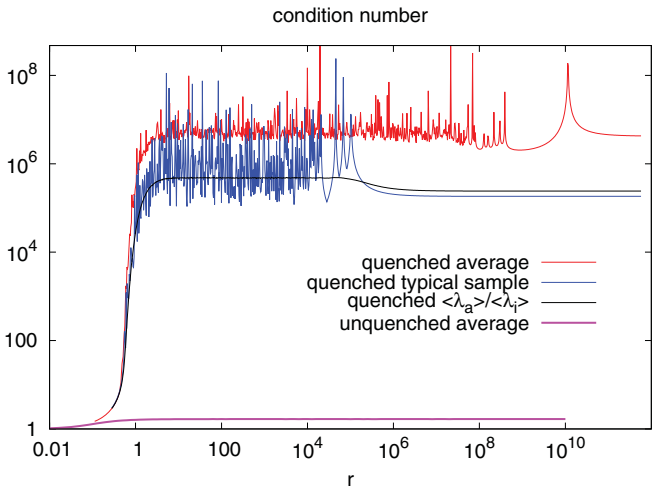

FIG. 3. (Color online) Condition number vs g for $\kappa = 0$ for a 32×16^3 lattice. The quenched average over 8692 samples is shown in red (upper curve), and a typical quenched sample is shown in blue (lower curve). For comparison the ratio $\frac{|\lambda_a|}{|\lambda_i|}$ is also shown in black. The results of the unquenched Monte Carlo simulation are denoted by the thick purple line.

plotted the average condition number without the quenched approximation: this is discussed in the next section.

In conclusion of this section, the size effects on this model for $\kappa = 0$ appear extremely severe: for any fixed value of g the occurrence of configurations with arbitrarily small eigenvalues in absolute value grows with size. This is reminiscent of the so-called exceptional configurations which have been encountered in the context of quenched lattice QCD [12].

C. Case $0 < \theta < \frac{\pi}{2}$

This region is nontrivial since the Dirac operator cannot be diagonalized as in the two previous cases. Nevertheless, this is where the physics takes place. As was done in Ref. [6,13–15], to perform a realistic calculation one finds the critical line, and one chooses the particular point close to this line where the ratio of the renormalized masses of fermions and bosons is equal to the physical one. This program has been done successfully, giving consistent results for small g. However, for g around 0.7, the linear system becomes ill conditioned to solve, preventing any conclusive result.

To illustrate the evolution of the spectrum in the parameter space, we have fully diagonalized the Dirac operator for an 8^4 lattice for the same typical field configuration. This is only possible within the quenched approximation where the probability of a field configuration is independent of κ and g. Figure 4 shows the spectra in the complex plane for $\mu = 0.3$ and θ ranging from $\frac{\pi}{2}$ to zero. The spectrum in Fig. 4(a) is close to the critical κ of the well-known free case (each point is highly degenerated, up to 768). Going from the spectrum in Fig. 4(a) to that in Fig. 4(f), the eigenvalues which are clustered for small g (exactly degenerated for $g = 0$) spread out. At the same time the imaginary part diminishes down to zero for $\kappa = 0$. Note that all these six spectra have been chosen close to an ill-conditioned case.

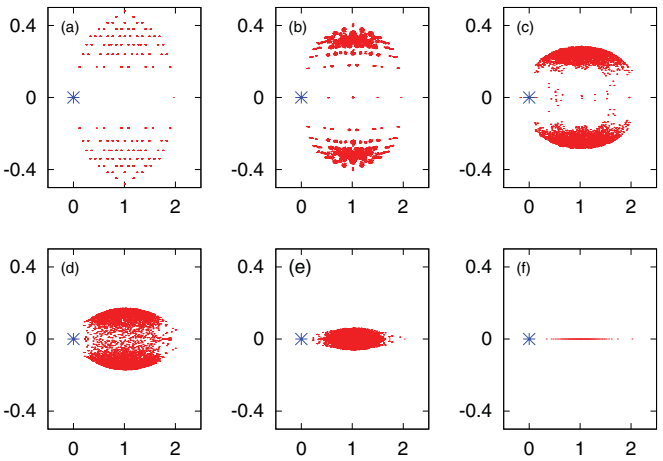

FIG. 4. (Color online) Full spectrum in the complex plane of the Dirac operator for (a) $(g,\kappa) = (0.005,0.120)$, (b) $(g,\kappa) = (0.427,0.114)$, (c) $(g,\kappa) = (0.771,0.101)$, (d) $(g,\kappa) = (0.8,0.070)$, (e) $(g,\kappa) = (0.8,0.035)$, and (f) $(g,\kappa) = (0.8,0)$, with $L = 8$ and $\mu = 0.3$. The origin is marked by a star.

We have computed the condition number for a field configuration for a 16^4 lattice in the region $0 \leqslant \kappa \leqslant 0.14$ and $0 \leqslant g \leqslant 0.8$. The results are presented in Fig. 5. An ill-conditioned region appears when g is larger than a value around 0.6 and for any κ, where large fluctuations of the condition number take place. For small g, it was shown in Ref. [6] that the critical line, defined as the line where the renormalized mass of the fermion vanishes, is a parabola originating from the point $\kappa = \frac{1}{8}, g = 0$. We therefore expected a diverging condition number along this line. This is clearly seen in Fig. 5. The localization of the ill-conditioned region for small κ agrees with what we have shown in Sec. II B for $\kappa = 0$ and confirms the huge size effects predicted. There is no reason to believe that these size effects are restricted to the $\kappa = 0$ line as suggested by the evolution of the spectrum between Figs. 4(e) and 4(f). The extent of this problematic region cannot be determined numerically, at least with present methods.

We see three possible origins for this problematic region. It can be that quenched approximation does not work for those values of g. This seems intuitively reasonable since the determinant in Eq. (6) precisely gives a low weight to these configurations with a large condition number. Another possible reason could be the specific choice of the action and the discretization of the fermion. Finally, there is the possibility that this is a fundamental problem of the Yukawa model without a direct meson-meson coupling term in the action.

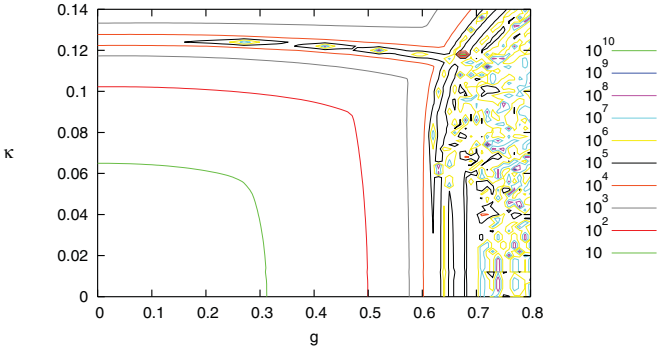

FIG. 5. (Color online) Isocondition number line on a 16^4 lattice.

III. THE $\kappa = 0$ CASE WITHOUT THE QUENCHED APPROXIMATION

In this section we consider the simple case $\kappa = 0$ as in Sec. II B, but *without* the quenched approximation. The purpose is to illustrate in this simple case the consequence of the quenched approximation. Intuitively the determinant in the probability density equation (6), gives a vanishing weight to the ill-conditioned configurations. So we can expect that the configurations to be included in the sampling will not have a large condition number. But it is possible to have a large determinant and still a small eigenvalue, for example if one eigenvalue is small and all the others are large. These configurations would have a nonvanishing weight, but still a very large condition number.

The joint probability of the fields ϕ_x, Eq. (6), can be written as

$$\Pi(\{\phi_x\}) \sim \exp\Bigg(-\frac{1}{2}\sum_x \Big[(8+\mu^2)\phi_x^2 - 2\sum_\mu \phi_{x+\mu}\phi_x\Big] + 4\ln|1+g\phi_x|\Bigg). \tag{23}$$

Since this expression cannot be factorized we can no longer generate independently a properly chosen combination of ϕ_x's. Instead, to generate the ϕ_x's, we have written two algorithms, one relying on the Monte Carlo method and the other on the heat-bath method.

A. Monte Carlo method

For the Monte Carlo method we use the simple Metropolis algorithm [16]. The normalization factor of Eq. (23) is very difficult to compute, but the ratio of the probability of two ϕ configurations is very simple to compute. The Monte Carlo method uses this fact to construct a Markov chain which has the desired distribution as a fixed point. In practice, we start from a initial ϕ_x configuration; then we choose at random a site x and try to change the value of ϕ_x for $\phi_x + d\phi$, where $d\phi$ is a random number normally distributed. We accept this change with the probability $\min(1, \exp -\Delta E)$, where E is the argument of the exponential in Eq. (23). We do not have a proof that this algorithm converges, the difficulty being that the number of states of the Markov chain is infinite. However, for all practical purpose it works properly if one always chooses as a starting distribution for a value g an equilibrium distribution for a close smaller value, $g - \delta g$. This indicates that the energy landscape is complicated, probably with metastable states. This naive algorithm is much simpler than the well-known hybrid Monte Carlo algorithm [10], but it is sufficient for our purpose. We have compared the two algorithms and find that the hybrid Monte Carlo algorithm is more efficient than the naive Monte Carlo algorithm if the parameters are properly chosen, but they both give the same results with a good accuracy.

B. Heat-bath method

We have also used a heat-bath method. The method is similar to the Monte Carlo method: one chooses randomly a site x and updates the corresponding ϕ_x. The new value is simply chosen according to its probability density, knowing the ϕ's on the neighboring sites. Note that the new value does not depend on the old value. This density probability is

$$f_\Phi(\phi) = K(1+g\phi)^4 \exp(-A\phi^2 + \phi s), \tag{24}$$

where K is the normalization factor, $A = \frac{8+\mu^2}{2}$, and s is the sum of the ϕ's of the neighboring sites. It is convenient since the integrated density of states takes the form

$$F_\Phi(\phi) = \frac{1}{2}\left[1 + \mathrm{erf}\left(\frac{2A\phi - s}{2\sqrt{A}}\right)\right] - \sqrt{\frac{A}{\pi}}\frac{P}{C} g \exp\left[-\left(\frac{2A\phi - s}{2\sqrt{A}}\right)^2\right], \tag{25}$$

where C and P are polynomials in A, g, s, and ϕ; P has degree 3 in ϕ and C does not depend on ϕ. The actual expressions are simple but tedious. It is then simple to draw a uniform random number in the interval [0,1] and to invert Eq. (25) by dichotomy to find ϕ. Under the same restrictions as for the Monte Carlo method, the heat-bath algorithm properly samples the distribution of the ϕ's.

C. Mean field approximation and small-g expansion

Before analyzing the condition number, let us look at the mean value $\langle\phi\rangle$ (vacuum expectation value). Recall that in the quenched approximation, due to the symmetry of Eq. (10) the average value $\langle\phi\rangle$ is zero. In the unquenched case it is simple to compute $\langle\phi\rangle$ in the mean field approximation, which consists of assuming that all the neighboring sites of the considered site have the mean value. An autocoherent equation is obtained by setting $s = 8\langle\phi\rangle$ in $\langle\phi\rangle = \int \phi f_\Phi(\phi) d\phi$, where $f_\Phi(\phi)$ is given by Eq. (24). This yields a fifth-degree polynomial. The mean value $\langle\phi\rangle$ is the properly chosen root of this polynomial. The coefficients of this polynomial are themselves polynomials in g and μ of degree up to 10. There is no difficulty in solving these polynomials, and the result is shown in Fig. 6. In the limit of g going to infinity (and $\mu^2 < 32$), one gets

$$\langle\phi\rangle_{\mu,g=\infty} = \frac{\sqrt{(8+\mu^2)(-3\,\mu^2 + 16 + \sqrt{6\,\mu^4 + 256})}}{8\mu}. \tag{26}$$

In the other limit, a small-g expansion of Eq. (23) yields

$$\langle\phi\rangle_{\mu,g} = 4g\sum_y \langle\phi_x\phi_y\rangle_{g=0} + O(g^3) = \frac{4g}{\mu^2} + O(g^3). \tag{27}$$

The same expression is also obtained in the mean field approximation above.

D. Results

Our unquenched results for $\kappa = 0$ are displayed in Fig. 6. The calculations have been done on a 16^4 lattice. Starting from a configuration $\phi_x = 0$ for any site x and $g = 0$, one performs iterations with both methods until equilibrium is reached and sufficient statistical data are collected; then g is slightly increased and the process is repeated.

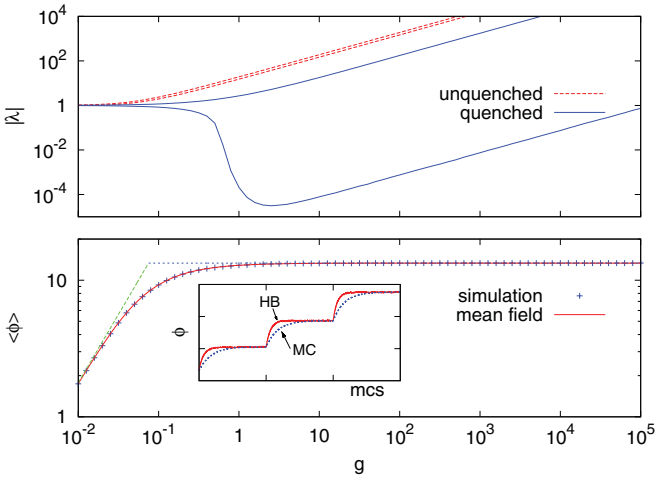

FIG. 6. (Color online) $|\lambda_{\min}|$ and $|\lambda_{\max}|$ in both a quenched and an unquenched simulation for $\kappa = 0$ (top), and $\langle\phi\rangle$ as a function of g (bottom). The points are the numerical results (heat-bath and Monte Carlo approaches are indistinguishable). The solid red line corresponds to the mean field. The horizontal dashed blue line corresponds to Eq. (26), and the dashed green line to the small-g expansion.

The lower part of Fig. 6 shows the mean value $\langle\phi\rangle$. The results obtained by the two numerical methods, shown as points, are indistinguishable. The mean field approximation is the straight line. We find an excellent agreement and conclude that both numerical methods converge and that the mean field approximation is quite good.

To evaluate the performance of the two numerical methods we show in the inset the average value of ϕ as a function of the number of steps. The value of g is changed at the end of each plateau. It is clear that the red solid line corresponding to the heat bath reaches the plateau before the dashed blue line corresponding to the Monte Carlo method. This indicates that the heat-bath method reaches equilibrium before the Monte Carlo method.

The results shown above indicate that we have properly sampled the distribution of ϕ's, and we can analyze the behavior of the condition number. Since the average $\langle\phi\rangle$ grows with g, it seems likely that $\min(|1+g\phi|)$ will not easily become small. This is indeed confirmed in the upper part of Fig. 6, where we have plotted the eigenvalues of minimum and maximum moduli for both the quenched and unquenched cases. It is clearly seen that $\lambda_{\min}$ is never small. Finally, the average condition number is plotted in Fig. 3, where the drastic effect of the quenched approximation is clearly seen: a reduction by six orders of magnitude of the condition number. This reduction is larger with larger lattices. We conclude that there is no ill-conditioned point on this $\kappa = 0$ line without the quenched approximation, whereas it is ill conditioned everywhere in the quenched approximation.

IV. SUMMARY AND PERSPECTIVES

We have analyzed in this paper the appearance of very small eigenvalues of Dirac operator in a Yukawa theory with Wilson fermions. The results obtained lead to the conclusion that, at finite volume and within the quenched approximation, these small eigenvalues are present in an entire region of the phase space. This indicates the existence of an ill-conditioned region, not just an ill-conditioned line; for example, the entire $\kappa = 0$ line is ill conditioned in the quenched approximation. Moreover, the size effects are exponentially large and consequently a numerical calculation can give apparently correct results, which would not survive the infinite volume limit. In other words, it does not seem possible to determine numerically the ill-conditioned region. The origin of this difficulty could be simply the choice of the discretization, or it could be the nonvalidity of the quenched approximation. This hypothesis is supported by an unquenched calculation for $\kappa = 0$ that is nowhere ill conditioned. But it could also be a problem of the Yukawa model itself. Indeed the Yukawa model is not a gauge model and there is no protection against spurious low eigenvalues like in QCD [12].

In this context we feel that the model should be studied without the quenched approximation to extend the result presented in this paper for the $\kappa = 0$ line. However, a boson self-coupling term $\lambda\phi^4$ has to be added to the Lagrangian to ensure renormalizability. This work is in progress.

ACKNOWLEDGMENTS

We acknowledge J. Carbonell, M. Papinutto, and O. Pene for many scientific discussions. This work was partially financed by Spanish Project No. FIS2010-18256.

APPENDIX: AVERAGE OF EXTREME EIGENVALUES FOR $\kappa = 0$

In this Appendix we show Eqs. (21) and (22). Since ϕ_x are normally distributed with zero mean and variance σ given by Eq. (12), the integrated probability distribution of $|\lambda|$ is

$$F_{|\lambda|}(|\lambda|) = \frac{1}{2}\left[\mathrm{erf}\left(\frac{|\lambda|-1}{\sqrt{2}g\sigma}\right) + \mathrm{erf}\left(\frac{|\lambda|+1}{\sqrt{2}g\sigma}\right)\right],$$

where σ is the variance of ϕ_x. Then from the definition of the minimum and after an integration by parts, one gets

$$\langle|\lambda_{\min}|\rangle = \int_0^\infty [1 - F_{|\lambda|}(x)]^N dc, \tag{A1}$$

$$\langle|\lambda_{\max}|\rangle = \int_0^\infty 1 - [F_{|\lambda|}(x)]^N dx. \tag{A2}$$

Introducing $\phi(y) = 1 - F_\sigma(y)$ we have

$$\langle\lambda_{\min}\rangle = \frac{1}{N}\int_0^\infty \left[\phi\left(\frac{y}{N}\right)\right]^N dy.$$

Since

$$\phi(h) = 1 - \sqrt{\frac{2}{\pi}}\frac{1}{g\sigma}\exp -\frac{1}{2g^2\sigma^2}h + O(h^3),$$

then

$$\phi\left(\frac{x}{N}\right)^N \to \exp\left(-x\sqrt{\frac{2}{\pi}}\frac{1}{g\sigma}e^{-\frac{1}{2g^2\sigma^2}}\right).$$

So

$$N\lambda_{\min} = \int_0^\infty \exp\left(-x\sqrt{\frac{2}{\pi}}\frac{1}{g\sigma}e^{-\frac{1}{2g^2\sigma^2}}\right)dx,$$

yielding Eq. (19).

We now study the behavior of $\lambda_{\max}$. When N is large the integrand in Eq. (A2) tends to a step function equal to 1 for $x < x^\star$ and equal to 0 for $x > x^\star$. One can estimate $x^\star$ as the unique zero of the second derivative of the integrand. Since $x^\star$ grows when N grows, one can replace $x - 1$ and $x + 1$ by x in the equation $\frac{d^2}{dx^2}F_{|\lambda|}(x)^N = 0$, yielding the equation

$$N = \sqrt{\frac{\pi}{2}}\frac{\langle\lambda_{\max}\rangle}{g\sigma}\exp\frac{1}{2}\left(\frac{\langle\lambda_{\max}\rangle}{g\sigma}\right)^2,$$

from which Eq. (22) follows.

[1] Jean Zinn-Justin, *Quantum Field Theory and Critical Phenomena* (Oxford University Press, New York, 2002).
[2] F. J. Dyson, Phys. Rev. **85**, 631 (1952).
[3] L. I. Schiff, Phys. Rev. **92**, 766 (1953); K. G. Wilson, Rev. Mod. Phys. **55**, 583 (1983).
[4] H. J. Rothe, *Lattice Gauge Theory*, Lecture Notes in Physics, Vol. 74 (World Scientific, Singapore, 2005).
[5] H. Yukawa, Proc. Math. Soc. Jpn. **17**, 48 (1935).
[6] F. de Soto, J. C. Anglès d'Auriac, and J. Carbonell, Eur. Phys. J. A **47**, 57 (2011).
[7] I.-H. Lee, J. Shigemitsu, and R. E. Shrock, Nucl. Phys. B **330**, 225 (1990).
[8] P. Gerhold and K. Jansen, J. High Energy Phys. 04 (2010) 094.
[9] I. Montvay and G. Munster, *Quantum Fields on a Lattice* (Cambridge University Press, Cambridge, England, 1994).
[10] S. Duane, A. D. Keneedy, B. J. Pendleton, and D. Roweth, Phys. Lett. B **195**, 216 (1987).
[11] Y. Saad, *Iterative Methods for Sparse Linear Systems*, 2nd ed. (SIAM, Philadelphia, 2003).
[12] H. Wittig, Nucl. Phys. B: Proc. Suppl. **119**, 59 (2003).
[13] F. de Soto, J. Carbonell, C. Roiesnel, Ph. Boucaud, J. P. Leroy, and O. Pene, Nucl. Phys. B: Proc. Suppl. **164**, 252 (2007).
[14] F. de Soto, J. Carbonell, C. Roiesnel, Ph. Boucaud, J. P. Leroy, and O. Pene, Eur. Phys. J. A **31**, 777 (2007).
[15] F. de Soto, J. Carbonell, C. Roiesnel, Ph. Boucaud, J. P. Leroy, and O. Pene, Nucl. Phys. A **790**, 410 (2007).
[16] N. Metropolis, A. W. Rosenbluth, M. N. Rosenbluth, A. H. Teller, and E. Teller, J. Chem. Phys. **21**, 1087 (1953).